Accurate screened QED calculations in high-Z many-electron ions

S. A. Blundell*
University of California, Lawrence Livermore National Laboratory, P.O. Box 808, Livermore, California 94550
(Received 6 March 1992)

We describe a practical, rigorous, QED procedure for performing accurate calculations of the screened self-energy for high-Z ions based on a realistic local atomic potential. Using a basis-set algorithm, we show that the procedure involves a rapidly convergent partial-wave expansion that, in contrast to previous methods, requires explicit computation of only the first few partial waves. We apply the method to the $2s$-$2p_{1/2}$ transition of Li-like U, the $3s$-$3p_{3/2}$ transition of Na-like Pt, and the $4s$-$4p_{1/2}$ transition in Cu-like Bi. When combined with calculations of the screened Uehling vacuum-polarization term and earlier correlation calculations, the results agree with experiment to within several tenths of an eV.

PACS number(s): 31.20.Tz, 12.20.Ds, 31.30.Jv

I. INTRODUCTION

While the evaluation of the radiative self-energy in high-Z ions has been definitively solved for point-nucleus hydrogenic ions [1–3], the evaluation of the self-energy, and QED corrections in general, for many-electron ions remains an outstanding problem in theoretical atomic physics. Yet interest in high-Z ions has grown considerably in recent years as experimental methods permit the study of higher charge states with greater precision. For example, a measurement of the resonance transition in Li-like U by Schweppe *et al.* [4] has achieved a precision of 0.09 eV (0.2% of the Lamb shift), and comparable precision has been obtained in Na-like Pt by Cowan *et al.* [5] and in Cu-like Th by Seely *et al.* [6]. In addition to providing data for modeling hot laboratory or astrophysical plasmas, these systems offer the possibility of making precision studies of a relativistic many-body system, bound by electromagnetism, in a regime in which radiative corrections are on a par with the electron-electron Coulomb interaction for determining the structure.

On the theoretical side, Johnson, Blundell, and Sapirstein [7–10] have recently applied relativistic many-body perturbation theory (RMBPT) to calculate highly converged correlation and Breit corrections for high-Z Li-like, Na-like, and Cu-like systems. By comparing with experiment, these authors inferred the QED effects omitted in their RMBPT calculations, finding them to be slightly smaller than those expected for hydrogenic ions, that is, corresponding to a reduced or "screened" nuclear charge. While several algorithms are available for estimating phenomenologically these screened QED effects (see for example Ref. [11]), a true test of QED requires an *ab initio* approach. The Feynman diagrams for the leading QED effects are shown in Fig. 1. In this paper we describe in detail a practical procedure for evaluating the largest and most difficult to calculate QED effect, the self-energy, in a realistic atomic potential.

While the formula for the bound-state self-energy and the general renormalization procedure have long been understood, the numerical evaluation for high Z has proved a hard problem. The early, largely analytical methods applied to hydrogen fail at moderate Z because it is no longer valid to expand in the parameter $Z\alpha$ that measures the strength of the nuclear Coulomb potential; what is needed instead is a direct numerical evaluation of the Feynman diagram. The first such correct calculation we believe was by Desiderio and Johnson [12] using a method suggested by Brown, Langer, and Schaefer [13]. With an improved algorithm, Mohr [1, 2] then solved the problem definitively for states in point-nucleus hydrogenic ions with principal quantum numbers $n = 1$ and $n = 2$; this work has recently been extended to $n = 3$–5 by Mohr and Kim [3].

A principal numerical problem in both these approaches, however, is a rather slowly convergent partial-wave expansion with asymptotic form $1/L^2$. Mohr calculated very precise results by introducing special functions specific to the point-nucleus Coulomb problem, and was able to extend the partial-wave expansion to an L value of several thousand. However, his numerical approach does not generalize immediately to an arbitrary potential. Recently, Indelicato and Mohr [14] have considered the linear effect on the Coulomb self-energy of a small additional screening potential. This approach may be expected to lose accuracy at low or intermediate Z, or for systems with more than a few electrons,

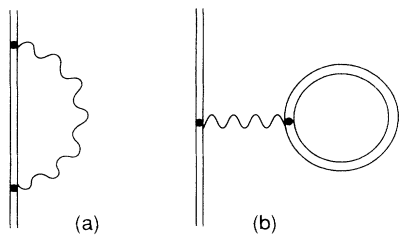

FIG. 1. Feynman diagrams for the lowest-order bound-state self-energy (a) and vacuum polarization (b). Double lines represent propagation in the external potential $V(r)$.

where the screening potential is not small compared to the nuclear Coulomb potential. Also the method cannot account for a finite nuclear charge distribution. A complete calculation of the self-energy for excited states in a non-Coulomb potential was recently given by Cheng, Johnson, and Sapirstein [15] using the original Brown *et al.* algorithm with improved numerical techniques and computing power. They were able to account for the bulk of the screening of the Lamb shift in selected Li-like, Na-like, and Cu-like systems, though with a numerical precision worse than the best experimental precision for high Z.

Here we describe an alternative approach to the problem of computing the self-energy in a non-Coulomb potential that we believe has important computational advantages. Our procedure is based partly on a recent suggestion by Snyderman [16], the essence of which is shown in Fig. 2. As in the early treatment of Baranger, Bethe, and Feynman [17], the electron propagator is expanded in terms of the total external potential $V(r) = V_{\rm nuc}(r) + V_{\rm scrn}(r)$, obtaining divergent zero- and one-potential terms, and a finite many-potential term. The divergences of the former two terms cancel against each other and the mass counterterm, leaving finite residues. While Baranger, Bethe, and Feynman extracted the physical self-energy through order $\alpha(Z\alpha)^5 mc^2$, Snyderman has suggested a numerical evaluation to all orders in $Z\alpha$ and $\ln(Z\alpha)$. He has given analytical expressions for the finite parts of the zero- and one-potential terms in the form of one- and three-dimensional momentum-space integrals, respectively; we here apply these expressions directly. For the many-potential term, we introduce a basis-set algorithm, which we use to examine the partial-wave expansion of this term. We find a relatively rapid convergence, roughly as $1/L^3$, that permits accurate evaluation of the self-energy with $L \leq 9$ for a single state; we find that even fewer partial waves are required for the self-energy of a transition. It follows that the slower $1/L^2$ convergence of the earlier methods is associated with the finite part of the one-potential term, which is here evaluated in momentum space. This is an important observation for self-energy calculations, because with such low partial waves sufficing, it is as easy to evaluate the self-energy for an arbitrary potential as it is for a Coulomb potential.

The first results of the method have already been presented in a Rapid Communication [18] with Snyderman. There we showed that the procedure gives precise agreement with the point-nucleus $1s$ self-energies of Mohr [1]. The present paper explains some of the details of that work, together with the extension to nonhydrogenic systems and a discussion of the finite-nuclear-size effect on the self-energy.

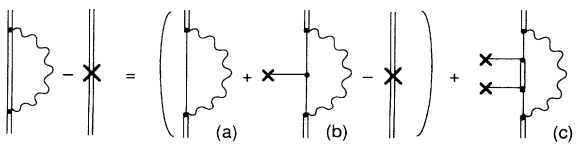

FIG. 2. Decomposition of the bound-state self-energy into (a) zero-, (b) one-, and (c) many-potential terms. Single lines represent free-electron propagators, double lines bound-electron propagators; solid lines terminated by a cross represent the binding potential $V(r)$.

The paper is organized as follows. In Sec. II we outline the formalism with emphasis on the basis-set algorithm for the many-potential term. We describe the most important numerical details in Sec. III. In the following section, we give three illustrative calculations for Li-like, Na-like, and Cu-like ions, which enable us to compare both to previous screening calculations and to experiment. For the latter purposes we calculate also screening corrections to the Uehling term of the vacuum polarization. In the final section we discuss prospects for improving the accuracy further, and for evaluating higher-order QED terms.

II. FORMALISM

We shall assume the electron-electron interaction to be approximated in the first instance by a suitable central potential $V_{\rm scrn}(r)$. By using a Furry representation of QED in the total potential $V(r) = V_{\rm nuc}(r) + V_{\rm scrn}(r)$, one can then develop a systematic perturbative expansion around $V(r)$ that contains in a consistent way both the correlation effects considered in the RMBPT approach and the residual QED effects [19]. We consider here the leading one-photon radiative corrections in such an approach, and require, therefore, that the electron wave functions and propagators refer to the potential $V(r)$.

The screening potential $V_{\rm scrn}(r)$ should ideally be some form of numerically generated self-consistent potential. For the method to be presented here to be fully consistent, however, $V_{\rm scrn}(r)$ must be a local potential. This restriction rules out direct use of a Dirac-Fock potential, but can admit local approximations to a Dirac-Fock potential. We in fact use the direct part of the Dirac-Fock potential in Sec. IV.

The radiative self-energy level shift of a single-particle state A with energy ε_A is given in the Furry picture by the real part of [17, 20]

$$E_{\rm SE} = \int d\mathbf{r}_1\, d\mathbf{r}_2\, \bar{\psi}_A(\mathbf{r}_2)\Sigma(\varepsilon_A;\mathbf{r}_2,\mathbf{r}_1)\psi_A(\mathbf{r}_1) - \delta m \int d\mathbf{r}\, \bar{\psi}_A(\mathbf{r})\psi_A(\mathbf{r}), \tag{1}$$

where δm is the free-electron mass shift, and $\Sigma(\varepsilon;\mathbf{r}_2,\mathbf{r}_1)$ is the bound-state self-energy operator

$$\Sigma(\varepsilon;\mathbf{r}_2,\mathbf{r}_1) = i\int_{-\infty}^{\infty}\frac{d\omega}{2\pi}\,\gamma_\mu G(\varepsilon-\omega;\mathbf{r}_2,\mathbf{r}_1)\gamma_\nu D^{\mu\nu}(\omega;\mathbf{r}_2,\mathbf{r}_1). \tag{2}$$

The quantities $D^{\mu\nu}(\omega;\mathbf{r}_2,\mathbf{r}_1)$ and $G(\varepsilon;\mathbf{r}_2,\mathbf{r}_1)$ here are

mixed-representation photon and bound-electron propagators that are discussed further below. To isolate and cancel the divergences appearing in (1), we follow the procedure of Refs. [16] and [17], which we sketch as follows. The bound-electron propagator G is expanded in terms of the binding potential according to Fig. 2. Inserting this form for G into (1) and (2), and converting to momentum space, gives

$$E_{\rm SE} = \int \frac{d\mathbf{p}}{(2\pi)^3}\,\bar\psi_A(\mathbf{p})\Sigma^{(0)}(\varepsilon_A,\mathbf{p})\psi_A(\mathbf{p}) + \int \frac{d\mathbf{p}_1}{(2\pi)^3}\frac{d\mathbf{p}_2}{(2\pi)^3}\,\bar\psi_A(\mathbf{p}_2)\Lambda^{(0)}_\mu(\varepsilon_A,\mathbf{p}_2;\varepsilon_A,\mathbf{p}_1)\psi_A(\mathbf{p}_1)\,V^\mu(\mathbf{p}_2-\mathbf{p}_1) + E_{\rm MP} - \delta m\int \frac{d\mathbf{p}}{(2\pi)^3}\,\bar\psi_A(\mathbf{p})\psi_A(\mathbf{p}). \tag{3}$$

This decomposition isolates the divergences in the free-electron self-energy $\Sigma^{(0)}$, the free-electron vertex function $\Lambda^{(0)}_\mu$, and the mass counterterm δm, while the residual many-potential term $E_{\rm MP}$ (developed below) is finite. Note that the one-potential term involves the Fourier transform of the local binding potential $V^\mu(r) = (V(r),\mathbf{0})$. The divergences can be displayed formally by means of the standard identities to $O(\alpha)$ [21]

$$\Sigma^{(0)}(p) = \delta m + (p^\mu\gamma_\mu - mc^2)(1-Z_2^{-1}) + \Sigma^{(0)}_{\rm fin}(p), \tag{4}$$

$$\Lambda^{(0)}_\mu(p_2,p_1) = \gamma_\mu(Z_1^{-1}-1) + \Lambda^{(0)}_{\mu,\rm fin}(p_2,p_1). \tag{5}$$

Upon substitution into (3), the first term in (4) cancels the mass counterterm, leaving terms dependent on the divergent renormalization constants Z_1 and Z_2. By virtue of the Fourier transform of the Dirac equation,

$$(p^\mu\gamma_\mu - mc^2)\psi(\mathbf{p}) = \int \frac{d\mathbf{q}}{(2\pi)^3}\,\gamma_\mu V^\mu(\mathbf{p}-\mathbf{q})\psi(\mathbf{q}), \tag{6}$$

and the free-electron Ward identity $Z_1 = Z_2$, however, these divergences cancel each other, and the final expression for the self-energy is given by a sum of three finite terms

$$E_{\rm SE} = \int \frac{d\mathbf{p}}{(2\pi)^3}\,\bar\psi_A(\mathbf{p})\Sigma^{(0)}_{\rm fin}(\varepsilon_A,\mathbf{p})\psi_A(\mathbf{p}) + \int \frac{d\mathbf{p}_1}{(2\pi)^3}\frac{d\mathbf{p}_2}{(2\pi)^3}\,\bar\psi_A(\mathbf{p}_2)\Lambda^{(0)}_{\mu,\rm fin}(\varepsilon_A,\mathbf{p}_2;\varepsilon_A,\mathbf{p}_1)\psi_A(\mathbf{p}_1)\,V^\mu(\mathbf{p}_2-\mathbf{p}_1) + E_{\rm MP}. \tag{7}$$

The finite parts of the self-energy and vertex functions, $\Sigma^{(0)}_{\rm fin}(p)$ and $\Lambda^{(0)}_{\mu,\rm fin}(p_2,p_1)$, are gauge dependent and depend also on the regularization scheme, but the sum (7) is gauge invariant and free of regularization ambiguities. In this work we use the explicit Feynman-gauge expressions for the zero- and one-potential terms derived by Snyderman [16] using dimensional regularization, with slight generalization to an arbitrary potential.

We now turn to the many-potential term shown in Fig. 3. The configuration-space Feynman rules give

$$E_{\rm MP} = i\int_{-\infty}^{\infty}\frac{d\omega}{2\pi}\int d\mathbf{r}_1 d\mathbf{r}_2 d\mathbf{r}_3 d\mathbf{r}_4\, D^{\mu\nu}(\omega;\mathbf{r}_1,\mathbf{r}_4)\bar\psi_A(\mathbf{r}_1)\gamma_\mu K(\varepsilon_A-\omega;\mathbf{r}_1,\mathbf{r}_2) \times\gamma_0 V(\mathbf{r}_2)G(\varepsilon_A-\omega;\mathbf{r}_2,\mathbf{r}_3)\gamma_0 V(\mathbf{r}_3)K(\varepsilon_A-\omega;\mathbf{r}_3,\mathbf{r}_4)\gamma_\nu\psi_A(\mathbf{r}_4), \tag{8}$$

where $K(\varepsilon;\mathbf{r}_2,\mathbf{r}_1)$ is the free-electron propagator. In the Feynman gauge used here, the photon propagator is [22]

$$D^{\mu\nu}(\omega;\mathbf{r}_2,\mathbf{r}_1) = \frac{g^{\mu\nu}}{|\mathbf{r}_2-\mathbf{r}_1|}\exp(i\sqrt{\omega^2+i\delta}\,|\mathbf{r}_2-\mathbf{r}_1|/c), \tag{9}$$

where δ is an infinitesimal positive quantity, and where the sign of the square root is chosen such that the argument to the exponential has a negative real part. For the free- and bound-electron propagators we use the eigenfunction representation,

$$K(\varepsilon;\mathbf{r}_2,\mathbf{r}_1) = \sum_\alpha \frac{\psi_\alpha(\mathbf{r}_2)\bar\psi_\alpha(\mathbf{r}_1)}{\varepsilon-\varepsilon_\alpha\pm i\delta}, \tag{10}$$

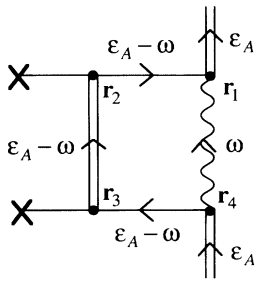

FIG. 3. Many-potential term. The energy arguments in Eq. (8) are given by energy conservation at each vertex.

$$G(\varepsilon;\mathbf{r}_2,\mathbf{r}_1)=\sum_i \frac{\psi_i(\mathbf{r}_2)\bar{\psi}_i(\mathbf{r}_1)}{\varepsilon-\varepsilon_i\pm i\delta}, \tag{11}$$

imagining the atom to be confined to a very large but finite cavity so that the spectrum of the Dirac Hamiltonian is discrete. Here and later, greek subscripts α, $\beta,\ldots$, refer to states of the free electron, and italic subscripts i, j, $\ldots$, to states in the binding potential $V(r)$. The sign of $i\delta$ in the denominator is positive for the positive-energy branch of the spectrum (including the discrete bound states), and negative for the negative-energy branch. Substituting (10) and (11) into (8) gives

$$E_{\rm MP}=i\int_{-\infty}^{\infty}\frac{d\omega}{2\pi}\sum_{\alpha,\beta,i}\frac{\langle A\beta|(\alpha_\mu)_1(\alpha_\nu)_2D^{\mu\nu}(\omega;12)|\alpha A\rangle\langle\alpha|V|i\rangle\langle i|V|\beta\rangle}{(\varepsilon_A-\omega-\varepsilon_\beta)(\varepsilon_A-\omega-\varepsilon_i)(\varepsilon_A-\omega-\varepsilon_\alpha)}, \tag{12}$$

where for notational simplicity we have left implicit the infinitesimal imaginary parts in the denominators. To reduce this expression to a form suitable for computation, we must perform the angular integrals analytically. We therefore express the free and bound single-particle states in spherical form,

$$\psi_i(\mathbf{r})=\begin{pmatrix} i\frac{1}{r}g_i(r)\chi_{\kappa_i m_i}(\hat{\mathbf{r}})\\ \frac{1}{r}f_i(r)\chi_{-\kappa_i m_i}(\hat{\mathbf{r}})\end{pmatrix}, \tag{13}$$

and use the spherical expansion for the outgoing-wave Green's function [23],

$$\frac{1}{|\mathbf{r}_2-\mathbf{r}_1|}\exp(ik\,|\mathbf{r}_2-\mathbf{r}_1|)=ik\sum_{L=0}^{\infty}(2L+1)j_L(kr_<)h_L^{(1)}(kr_>)\,C^L(\hat{\mathbf{r}}_1)\cdot C^L(\hat{\mathbf{r}}_2), \tag{14}$$

to derive a multipole expansion for the frequency-dependent photon interaction having the structure

$$\langle ab|(\alpha_\mu)_1(\alpha_\nu)_2D^{\mu\nu}(\omega;12)|cd\rangle=\sum_{L=0}^{\infty}J_L(abcd)R_L(\omega;abcd). \tag{15}$$

Here $J_L(abcd)$ gives the usual magnetic-substate dependence associated with a scalar two-body operator,

$$J_L(abcd)=\sum_{m_L}(-1)^{j_a-m_a+L-m_L+j_b-m_b}\begin{pmatrix} j_a & L & j_c\\ -m_a & m_L & m_c\end{pmatrix}\begin{pmatrix} j_b & L & j_d\\ -m_b & -m_L & m_d\end{pmatrix}, \tag{16}$$

while $R_L(\omega;abcd)$ is a frequency-dependent generalized Slater integral. An expression for $R_L(\omega;abcd)$ in Feynman gauge is given in Appendix A. After substituting (15) into (12), we perform the sums over magnetic substates with standard graphical techniques [24], finding

$$E_{\rm MP}=i\int_{-\infty}^{\infty}\frac{d\omega}{2\pi}\sum_{\kappa L}\Delta(j_i,j_A,L)\frac{(-1)^{j_A-j_i+L}}{(2j_A+1)}\sum_{n_\alpha,n_\beta,n_i}\frac{R_L(\omega;A\beta\alpha A)V_{\alpha i}V_{i\beta}}{(\varepsilon_A-\omega-\varepsilon_\beta)(\varepsilon_A-\omega-\varepsilon_i)(\varepsilon_A-\omega-\varepsilon_\alpha)}, \tag{17}$$

where the Dirac angular quantum number $\kappa=\kappa_\alpha=\kappa_\beta=\kappa_i$. The symbol $\Delta(j_i,j_A,L)$ is unity if the three angular momenta satisfy a triangular condition, and zero otherwise. The matrix element of the potential is given by

$$V_{ab}=\int_0^{\infty}dr\,V(r)[g_a(r)g_b(r)+f_a(r)f_b(r)]. \tag{18}$$

The poles and cuts for the photon-frequency integral in (17) are shown in Fig. 4. The photon propagator contributes cuts that pinch the origin, while the free- and bound-electron propagators contribute branch cuts (or poles in a cavity) on either side of the imaginary axis. The bound-electron propagator also gives a set of poles that crosses the imaginary axis, with one pole $i=A$ lying on the imaginary axis, and poles from states of lower energy than A to the right of this axis. To perform the ω integral numerically, we rotate the contour anticlockwise about $\omega=0$ to the imaginary axis, obtaining a principal-value integral, pole terms from states of lower

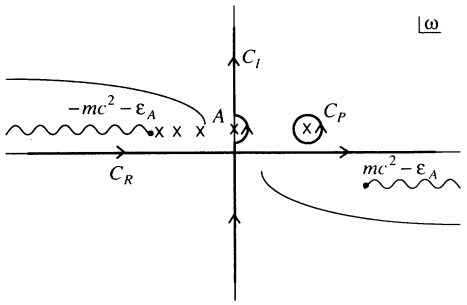

FIG. 4. Photon frequency-plane singularities for the many-potential term. Solid lines: photon-propagator branch cuts. Wavy lines: multiple branch cuts of free- and bound-electron propagators. Crosses: discrete poles of bound-electron propagator. The contour C_R is rotated anticlockwise to give C_I plus pole terms C_P.

energy than A, and a half-pole term from A itself,

$$E_{\rm MP} = E_{\rm PV} + \tfrac{1}{2}E^{(A)}_{\rm pole} + \sum_{i\ (\varepsilon_i<\varepsilon_A)} E^{(i)}_{\rm pole}. \tag{19}$$

The principal-value integral from the negative imaginary axis is the complex conjugate of that from the positive imaginary axis. Thus

$$E_{\rm PV} = -\frac{1}{\pi}\,{\rm Re}\sum_\kappa \int_0^\infty d\omega \sum_{L=0}^\infty \Delta(j_i,j_A,L)\frac{(-1)^{j_A-j_i+L}}{(2j_A+1)} \sum_{n_\alpha,n_\beta,n_i} \frac{R_L(i\omega;A\beta\alpha A)V_{\alpha i}V_{i\beta}}{(\varepsilon_A-i\omega-\varepsilon_\beta)(\varepsilon_A-i\omega-\varepsilon_i)(\varepsilon_A-i\omega-\varepsilon_\alpha)}. \tag{20}$$

A convenient way to organize the calculation of the principal-value term is to introduce a frequency-dependent effective basis state $\phi_i(i\omega)$,

$$|\phi_i(i\omega)\rangle = \sum_\alpha \frac{|\alpha\rangle\langle\alpha|\,V\,|i\rangle}{(\varepsilon_A - i\omega - \varepsilon_\alpha)}, \tag{21}$$

which can also be regarded as the solution to an inhomogeneous Dirac equation

$$(\varepsilon_A - i\omega - h_D)\,|\phi_i(i\omega)\rangle = V\,|i\rangle\,. \tag{22}$$

The principal-value term can then be evaluated as

$$E_{\rm PV} = -\frac{1}{\pi}\,{\rm Re}\sum_\kappa \int_0^\infty d\omega \sum_{L=0}^\infty \Delta(j_i,j_A,L)\frac{(-1)^{j_A-j_i+L}}{(2j_A+1)} \times \sum_{n_i} \frac{R_L(i\omega;A\phi_i\phi_i A)}{(\varepsilon_A-i\omega-\varepsilon_i)}. \tag{23}$$

The pole term from a state i with $\varepsilon_i < \varepsilon_A$ follows from (17) and (21) to be

$$E^{(i)}_{\rm pole} = \sum_{L=0}^\infty \Delta(j_i,j_A,L)\frac{(-1)^{j_A-j_i+L}}{(2j_A+1)} \times R_L(\omega;A\phi_i(\omega)\phi_i(\omega)A), \tag{24}$$

where $\omega = \varepsilon_A - \varepsilon_i$. This expression can be simplified with the identity $|\phi_i(\varepsilon_A-\varepsilon_i)\rangle = |i\rangle$, which follows from considering the difference between the eigenvalue equation for $|i\rangle$ and Eq. (22) with $i\omega = \varepsilon_A - \varepsilon_i$. The replacement of $\phi_i(\omega)$ by i in (24) shows that the pole terms of the many-potential term are identical to those for the whole self-energy discussed in Ref. [13]. The half-pole term for $i = A$ is obtained by taking one-half the above formula. A state i degenerate with A would also contribute a half-pole term, although this possibility would only occur in practice when $V(r)$ is a pure Coulomb potential, a case not considered explicitly here.

The self-energy for an excited state as defined by (1) is complex, with the imaginary part representing minus one half the one-photon decay rate of the excited state in a hydrogenic ion. In the present formalism, this imaginary part enters entirely through the pole terms $E^{(i)}_{\rm pole}$. The level shift considered here is given by the real part of the self-energy.

We also evaluate the leading part of the vacuum polarization, the Uehling term, by taking the atomic expectation value of the Uehling potential $U(\mathbf{r})$ [25, 26],

$$E_{\rm VP} = \int d\mathbf{r}\,\bar\psi_A(\mathbf{r})\gamma_0 U(\mathbf{r})\psi_A(\mathbf{r}), \tag{25}$$

where

$$U(\mathbf{r}) = -\frac{\alpha}{\pi}\int d\mathbf{r}'\,\rho(\mathbf{r}')\int_1^\infty dt\,(t^2-1)^{1/2}\left(\frac{2}{3t^2}+\frac{1}{3t^4}\right)\frac{\exp(-2ct\,|\mathbf{r}-\mathbf{r}'|)}{|\mathbf{r}-\mathbf{r}'|}, \tag{26}$$

with $\rho(\mathbf{r}')$ the charge distribution responsible for the total binding potential $V(r)$. Since $\rho(\mathbf{r}')$ here is spherically symmetric, only the $L = 0$ term contributes in a multipole expansion of the form (14), and we find

$$U(r) = -\frac{\alpha}{\pi}\int_0^\infty dr'\,(4\pi r'^2)\rho(r') \times \int_1^\infty dt\,(t^2-1)^{1/2}\left(\frac{2}{3t^2}+\frac{1}{3t^4}\right) \times \left[-2ct\,j_0(i2ctr_<)h_0^{(1)}(i2ctr_>)\right]. \tag{27}$$

A similar treatment of screening corrections to the Uehling term has been given by Cheng, Johnson, and Sapirstein [15] and Indelicato and Lindroth [27].

III. NUMERICAL DETAILS

We use Gaussian integration to evaluate the zero- and one-potential terms, and for the t integration in the Uehling potential. While the integration of the zero-potential term and the Uehling potential is straightforward, the one-potential term requires some care. This latter term has the structure [16]

$$\int_0^\infty d|\mathbf{p}_2|\int_0^\infty d|\mathbf{p}_1|\int_{-1}^1 dz\,\bar\phi_A(|\mathbf{p}_2|)\frac{1}{|\mathbf{p}_2-\mathbf{p}_1|^2}f(|\mathbf{p}_2|,|\mathbf{p}_1|,z)\phi_A(|\mathbf{p}_1|), \tag{28}$$

involving integration over the magnitudes of the vectors $\mathbf{p}_1$ and $\mathbf{p}_2$ and the cosine of the angle between them, $z = \cos\theta_{12}$. The integrand contains an integrable Coulomb singularity when $\mathbf{p}_1 = \mathbf{p}_2$, as well as a smooth function $f(|\mathbf{p}_2|, |\mathbf{p}_1|, z)$. The Coulomb singularity is readily handled by the set of variable transformations given in Appendix B; with this scheme we obtain six-figure accuracy with about 40–50 Gaussian points in each of the three dimensions. The function $f(|\mathbf{p}_2|, |\mathbf{p}_1|, z)$, however, involves an extra integration over a Feynman parameter x (so that the whole integral is effectively four-dimensional), the integrand of which contains spikes near the end of the integration range at $x = 0$ and $x = 1$. We therefore split the x integral into three parts, using Gaussian integration for each.

An additional complication is that the integrand of the zero- and one-potential terms contains the Fourier transform of the atomic wave function, the "radial" part of which involves a spherical Bessel transform of the form

$$\int_0^\infty dr\, r^2 j_L(pr) f_A(r), \tag{29}$$

where $f_A(r)$ is a radial configuration-space wave function. For an arbitrary binding potential $V(r)$, we must evaluate these transforms numerically. We start from the numerical configuration-space wave function and evaluate the transform by a direct point-by-point integration algorithm, reproducing the norm with an accuracy of at least 1 part in 10^8. We test the algorithm against the known analytic Coulomb transforms at each momentum point, finding satisfactory agreement of at least one part in 10^{10} for typical atomic values of momentum p, worsening to about one part in 10^4 for the large values $p \sim 100mc$ that make a small contribution to the integrals. We can further test the accuracy of our integration and Fourier-transform algorithms by considering the following test integrals:

$$\int \frac{d\mathbf{p}}{(2\pi)^3}\, \bar{\psi}_A(\mathbf{p})(p^\mu \gamma_\mu - mc^2)\psi_A(\mathbf{p}) = \langle V \rangle\,, \tag{30}$$

$$4\pi \int \frac{d\mathbf{p}_1}{(2\pi)^3} \frac{d\mathbf{p}_2}{(2\pi)^3}\, \bar{\psi}_A(\mathbf{p}_2)\gamma_0 \frac{\rho(\mathbf{p}_2 - \mathbf{p}_1)}{|\mathbf{p}_2 - \mathbf{p}_1|^2} \psi_A(\mathbf{p}_1) = \langle V \rangle\,, \tag{31}$$

where $\rho(\mathbf{q})$ is the Fourier transform of the charge density that generates $V(r)$. When evaluated with the same Gaussian points and momentum-space wave functions as the zero- and one-potential terms, the left-hand sides of the above equations equal $\langle V \rangle$ to within at worst a few parts in 10^6. From these tests we conclude that the accuracy of the zero- and one-potential terms is much better than that of the many-potential term discussed below.

The many-potential term is the most computationally expensive part of the calculation. The basic numerical tool we use to evaluate it is a relativistic finite basis set constructed from B splines [28]. In this method, we first confine the atom to a cavity of large radius, so that the spectrum of states is explicitly discrete as implied in Eqs. (10) and (11). We choose the cavity radius to be sufficiently large so as not to affect the numerical value of the self-energy at the required level. For $Z = 70$–90, we use a radius of 2–$3a_0$. The small and large components of the radial Dirac wave function for a given angular momentum κ are then expanded in terms of M piecewise polynomial or B-spline functions $B_i(r)$ [29]

$$\begin{pmatrix} g(r) \\ f(r) \end{pmatrix} = \sum_{i=1}^{M} \begin{pmatrix} c_i \\ d_i \end{pmatrix} B_i(r). \tag{32}$$

Following Ref. [28], the expansion coefficients are determined by minimizing the Dirac action, leading to a $2M \times 2M$ linear eigenvalue problem. The $2M$ solutions of this problem define a pseudospectrum, M states of which approximate the bound states and positive-energy continuum, and the remaining M the negative-energy continuum, of the unconfined particle. The lowest-lying states in the positive-energy branch of the pseudospectrum accurately reproduce the lowest-lying bound-state eigenfunctions and energies. Detailed tests of the accuracy and completeness of basis sets of this type are given in Ref. [28].

To implement the formulas for the many-potential term given earlier we need two separate basis sets, one for a free electron, and one for an electron in a potential $V(r)$. The free basis set is used to construct the effective basis functions $\phi_i(i\omega)$ from (21), a procedure essentially equivalent to solving the inhomogeneous Dirac equation (22) with the finite-element technique. The basis set in the potential $V(r)$ is used to sum over i in (23). Our justification for this latter use of the basis set is principally empirical. As far as we can tell, $E_{\rm PV}$ converges to a well-defined limit as the number of basis functions M is increased, and this limit agrees closely with self-energy results obtained using Green's-function techniques (see, for example, the close agreement with Mohr for $1s$ states reported in Ref. [18]). We note that both negative- and positive-energy basis states are important numerically. In our final calculations we use $M = 70$ basis states per κ value for a $1s$ self-energy, and about $M = 110$ for excited states. Empirically, we find that greater accuracy is obtained if the two separate basis sets have different numbers of states, with $M_V > M_{\rm free}$; in practice we choose $M_V = M_{\rm free} + 20$.

In the present work, the photon-frequency (ω) integral extends to a far greater upper limit (of order 10–$100mc^2$ for $1s$ states) than is necessary for analogous loop integrals in the relativistic correlation calculations to which the basis-set technique has so far been applied. We therefore improve the high-energy representation of the basis set by placing a large number of the "knot" points that define the B splines [29] close to the origin. We use an exponential distribution of knots, $r_i = a\{\exp[h(i-1)] - 1\}$, with the first nonzero knot point at distances of order $10^{-6}a_0$. For the free-electron basis set, we further improve accuracy by enforcing the boundary condition at the origin directly, rather than variationally as done in Ref. [28]. Our basis set does not work so well for the point-nucleus problem, because the Coulomb singularity in the wave function is not well represented by B splines. A point-nucleus calculation re-

quires knot points at even smaller radii, and generally more basis functions, than a finite-nucleus calculation of similar accuracy. We in fact find it more convenient to extrapolate a sequence of finite-nucleus calculations to zero nuclear size, as done previously [18].

We organize the calculation of the principal-value integral $E_{\rm PV}$ as indicated in Eq. (23), with the outermost loop over the angular momentum κ in the electron propagator. We group the values of κ corresponding to an orbital angular momentum l [that is $\kappa = l, -(l+1)$ for $l > 0$], and use Gaussian integration to perform the ω integral for each l, with a convenient transformation to map the infinite integration range to a finite one. About 15–20 Gaussian points then suffice for the accuracies obtained here. A special problem occurs when a state j appears in the sum over i in (23) that is nearly degenerate with the external state A, as can happen at high Z for states that would be degenerate for a Coulomb potential (e.g., $j = 2p_{1/2}$ for $A = 2s_{1/2}$), and at low Z for states separated only by fine structure (e.g., $j = 2p_{1/2}$

TABLE I. Self-energy of excited states of hydrogenlike Hg ($Z = 80$), after extrapolation to zero nuclear size following the procedure of Ref. [18]. Pole terms have been added on to the appropriate L-wave contribution (e.g., a $2s$ pole term to the $L = 0$ result). Units are rydbergs.

Term	Self-energy				
	$2p_{1/2}$	$2p_{3/2}$	$3s$	$3p_{1/2}$	$3p_{3/2}$
Zero potential	−17.177	−15.122	−8.660	−9.381	−8.657
One potential	10.400	9.279	6.357	6.292	5.841
Many potential					
$L = 0$	0.136	0.479	2.502	0.074	0.187
$L = 1$	6.307	5.155	0.319	2.695	2.350
$L = 2$	0.340	0.319	0.117	0.218	0.205
$L = 3$	0.111	0.107	0.055	0.080	0.076
$L = 4$	0.048	0.047	0.031	0.039	0.037
$L = 5$	0.025	0.025	0.019	0.022	0.021
$L = 6$	0.014	0.015	0.012	0.014	0.013
$L = 7$	0.009	0.009	0.008	0.009	0.009
$L = 8$	0.006	0.006	0.006	0.006	0.006
$L = 9$	0.004	0.004	0.004	0.005	0.005
Extrap. $L = 10 - \infty$	0.015(2)	0.015(2)	0.019(2)	0.018(2)	0.019(2)
Total many potential	7.015(2)	6.181(2)	3.093(2)	3.182(2)	2.930(2)
Total	0.238(2)	0.338(2)	0.789(2)	0.093(2)	0.114(2)
Other[a]	0.2386(4)	0.3383(5)	0.78879(4)	0.09319(4)	0.11401(4)
	$3d_{3/2}$	$3d_{5/2}$	$4s$	$4p_{1/2}$	$4p_{3/2}$
Zero potential	−9.223	−8.985	−5.708	−6.029	−5.688
One potential	6.216	6.099	4.266	4.263	4.038
Many potential					
$L = 0$	0.037	0.042	1.379	0.051	0.099
$L = 1$	0.222	0.234	0.200	1.470	1.326
$L = 2$	2.387	2.289	0.076	0.142	0.135
$L = 3$	0.191	0.186	0.038	0.054	0.052
$L = 4$	0.066	0.065	0.022	0.028	0.027
$L = 5$	0.032	0.031	0.014	0.016	0.016
$L = 6$	0.018	0.018	0.009	0.011	0.010
$L = 7$	0.011	0.011	0.007	0.007	0.007
$L = 8$	0.007	0.007	0.005	0.005	0.005
$L = 9$	0.005	0.005	0.004	0.004	0.004
$L = 10 - \infty$	0.019(2)	0.020(2)	0.018(2)	0.020(2)	0.019(2)
Total many potential	2.996(2)	2.909(2)	1.771(2)	1.808(2)	1.701(2)
Total	−0.012(2)	0.022(2)	0.330(2)	0.043(2)	0.051(2)
Other[a]	−0.01047(4)	b	0.32995(2)	0.04194(2)	0.05019(2)

[a] Mohr [2], and Mohr and Kim [3].

[b] Not previously calculated.

for $A = 2p_{3/2}$). In each case we find it better to separate the nearby state from the integrand, schematically,

$$E_{\rm PV} = \int_0^\infty d\omega\, F_j(\omega) + \int_0^\infty d\omega \sum_{i\ (\neq j)} F_i(\omega), \qquad (33)$$

and integrate the two parts separately using different sets of Gaussian points.

After truncating the κ sum at some $l_{\rm max}$, typically $l_{\rm max} = 9$, we extrapolate the l sum to infinity by fitting the partial-wave contributions to a polynomial in $1/l$,

$$E_{\rm PV}(l) = \frac{1}{l^n}\left(a_0 + \frac{a_1}{l} + \frac{a_2}{l^2} + \cdots\right). \qquad (34)$$

Some typical partial-wave summations are shown in Table I. The terms for $l = 7$–9 follow quite closely a $1/l^3$ dependence ($n = 3$ in the above). By considering fits with $n = 2$, 3, and 4, and with varying numbers of terms included, we find about a 10% variation in the extrapolated sum for $l = 10$–∞. This forms the leading numerical error in the calculation of the self-energy of a single state. While it is certainly possible to calculate to higher L, or to construct more sophisticated and accurate extrapolation schemes, we note that the error we can obtain in this way is already comparable to or better than typical experimental errors. For example, for $Z = 80$ we find an error of about 0.02 eV [18], while the most accurate experiments for $Z > 70$ also have a claimed accuracy of no better than about 0.02 eV [6]. Moreover, most experimental results of interest involve transitions between states with the same principal quantum number. In that case, the high-l part of the sum cancels very closely between the two states, and the self-energy of the transition is essentially free of the extrapolation error. In Table II we show the l convergence for a transition in Na-like Pt with a suboptimal basis set with $M = 90$. The quoted numerical error is the difference with the same calculation with $M = 70$, and is mostly basis-set truncation error. We see that not only the extrapolation error, but also most of the basis-set truncation error cancels systematically in the transition. From test calculations such as this, we find we can readily control the numerical error in the self-energy for these transitions to be ≤ 0.003 eV.

TABLE II. Screened self-energy calculation in Na-like Pt ($Z = 78$). Units are eV.

	Self-energy		
Term	$3s$	$3p_{3/2}$	$3p_{3/2}$-$3s$
Zero potential	−97.40	−96.95	0.452
One potential	72.55	67.05	−5.499
Many potential			
$L = 0$	26.85	1.83	−25.012
$L = 1$	3.18	25.20	22.020
$L = 2$	1.14	2.05	0.911
$L = 3$	0.53	0.74	0.208
$L = 4$	0.29	0.36	0.066
$L = 5$	0.18	0.21	0.027
$L = 6$	0.12	0.13	0.012
$L = 7$	0.08	0.09	0.006
$L = 8$	0.06	0.06	0.004
$L = 9$	0.04	0.04	0.002
$L = 10 - \infty$	0.17	0.18	0.006
Total many potential	32.64(6)	30.89(6)	−1.749(3)
Total self-energy	7.79(6)	0.99(6)	−6.796(3)

IV. APPLICATIONS

To illustrate the above procedure we consider three recent measurements on high-Z one-valence-electron systems: the $2s$-$2p_{1/2}$ transition of Li-like U measured by Schweppe *et al.* [4], the $3s$-$3p_{3/2}$ transition in Na-like Pt measured by Cowan *et al.* [5], and the $4s$-$4p_{1/2}$ transition in Cu-like Bi measured by Seely *et al.* [6]. The correlation, nuclear-finite-size, and Breit corrections to these transitions have previously been calculated by Johnson, Blundell, and Sapirstein [7–10] using RMBPT. The leading QED effects omitted in that work have been estimated phenomenologically by several authors [11,30–32], and only recently calculated in a rigorous QED approach by Indelicato and Mohr for Li-like U [14], and by Cheng, Johnson, and Sapirstein [15] for Li-like U and Na-like Pt. Here we show the results of our procedure compared both to the screened QED calculations of these authors, and to experiment.

The algorithm presented above can be applied to calculate two types of screening effect on the self-energy in these transitions: the screening of the valence self-energy by the mean potential of the core electrons, and the change in the total self-energy of the core electrons as they adjust to the different valence electrons of the transition. The screening of the valence self-energy represents a direct application of our formalism requiring only the specification of a suitable local screening potential. We choose the direct part of the V^{N-1} Dirac-Fock potential,

$$V_{\rm DF,dir}(r) = \sum_{c\ ({\rm core})} (2j_c + 1) \int_0^\infty dr' \frac{1}{r_>}[g_c^2(r') + f_c^2(r')], \qquad (35)$$

where g_c and f_c are radial eigenstates in the full V^{N-1} Dirac-Fock potential. The screening corrections we consider in this way are given in the linear approximation by the Feynman diagrams in Fig. 5. With this choice of screening potential, these diagrams are effectively absorbed into the lowest-order diagrams in Fig. 1, together with a higher-order set of diagrams that are nonlinear in the screening potential.

We should in principal recalculate the RMBPT correlation in this new potential. As Cheng, Johnson, and Sapirstein have shown, however, the highly converged correlation calculation is nearly independent of the choice of potential (as it would be exactly in the nonrelativistic limit), and we can take the Dirac-Fock correlation of Johnson, Blundell, and Sapirstein [7–9] with negligible error for our present purposes.

We calculate the second screening effect, the change of the core self-energy in the transition, by evaluating the

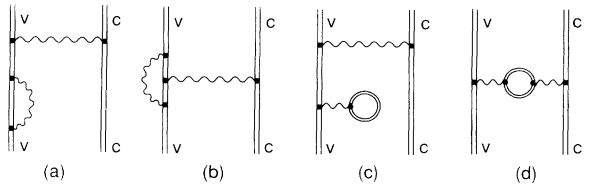

FIG. 5. Typical leading screening corrections to (a) and (b) the valence self-energy, and (c) and (d) the valence vacuum polarization. v, valence state; c, core state.

self-energy for each core state c in the state-dependent screening potential $V_c(r)$,

$$V_c(r) = \sum_a n_a \int_0^\infty dr' \frac{1}{r_>}[g_a^2(r') + f_a^2(r')]. \tag{36}$$

Here the sum over a extends over all orbitals occupied in the atom, including the valence state v, with n_a the occupation number of the orbital. We take $n_v = 1$, $n_a = 2j_a + 1$ for a core orbital $a \neq c$, and $n_c = 2j_c$ for the core orbital c under consideration. The potential $V_c(r)$ thus differs from $V_{\mathrm{DF,dir}}(r)$ by the addition of the spherically averaged potential of the valence electron, and the removal of the potential due to the core electron c itself, which would otherwise give a spurious self-interaction. We take as the contribution to the transition energy for $v \to w$

$$\Delta E_{\mathrm{SE,core}} = \sum_{c\ (\mathrm{core})} (2j_c + 1)\left[E_{\mathrm{SE}}^{(w)}(c) - E_{\mathrm{SE}}^{(v)}(c)\right], \tag{37}$$

where $E_{\mathrm{SE}}^{(v)}(c)$ is the self-energy of c with a valence electron v present. The leading Feynman diagrams for this "core-relaxation" effect are shown in Fig. 6. In the linear approximation of this figure, the core terms in the potential (36) cancel identically in the transition (37) leaving only the effect of the valence potential. Our method includes this lowest-order term, plus an approximation to a higher-order set of terms in which cross terms between the valence and core parts of the screening potential enter.

We also calculate the screened Uehling term from (25) and (27) for both the valence and the core using a procedure analogous to that described above for the self-energy. To complete the calculation of the lowest-order vacuum polarization, we add the small Wichmann-Kroll (WK) terms by scaling the hydrogenic values tabulated by Johnson and Soff [33] or by Soff and Mohr [34]. We assume here that the WK terms scale in the same way as the Uehling term.

We now turn to the $2s_{1/2}$-$2p_{1/2}$ transition of Li-like U. Our first step is to consider the self-energy of this transition for a *hydrogenic* ion with a finite nucleus, modeled by a Fermi distribution with an rms radius $\langle r^2\rangle^{1/2} = 5.863$ fm [35]. The zero-, one-, and many-potential terms are shown in Table III. Comparing with the point-nucleus result of Mohr [2], -56.670 eV, we infer a finite-size correction to the hydrogenic self-energy of

TABLE III. Self-energy and Uehling terms for the $2s$ and $2p_{1/2}$ states in hydrogenlike U ($Z = 92$) with a finite nucleus. Units are eV.

	Energy		
Term	$2s$	$2p_{1/2}$	$2p_{1/2}$-$2s$
Zero potential	−252.87	−293.26	−40.39
One potential	193.21	173.69	−19.52
Many potential			
$L = 0$	107.89	0.57	−107.31
$L = 1$	10.51	118.67	108.16
$L = 2$	3.40	5.85	2.45
$L = 3$	1.40	1.94	0.54
$L = 4$	0.69	0.84	0.15
$L = 5$	0.38	0.43	0.05
$L = 6$	0.23	0.24	0.02
$L = 7$	0.15	0.15	0.00
$L = 8$	0.10	0.10	0.00
$L = 9$	0.07	0.07	0.00
$L = 10 - \infty$	0.24	0.24	0.00
Total many potential	125.05(6)	129.10(6)	4.05(1)
Total SE	65.39(6)	9.52(6)	−55.87(1)
Uehling	−16.46	−2.91	13.56

0.80(1) eV, which is therefore experimentally observable (about 9 experimental standard deviations). This value for the finite-nuclear-size correction lies about halfway between the results of Johnson and Soff [33], 1.0(1) eV, and of Cheng, Johnson, and Sapirstein [15], 0.6(2) eV, broadly agreeing with both within one to two experimental standard deviations. We note that in another calculation of the finite-size correction to the self-energy, for the $1s$ self-energy in hydrogenlike Hg, we disagree with Johnson and Soff, finding 1.13(6) eV compared to their value 1.63(15) eV. However, in this case we agree with an unpublished result of Cheng, Johnson, and Sapirstein [36].

As a second step, we consider in Table IV the screened valence self-energy in Li-like U. We find $-54.09(1)$ eV for the transition. Comparing with our finite-nucleus hydrogenic value, $-55.87(1)$ eV, we infer a "valence screening" correction of 1.77(1) eV for the transition. This value

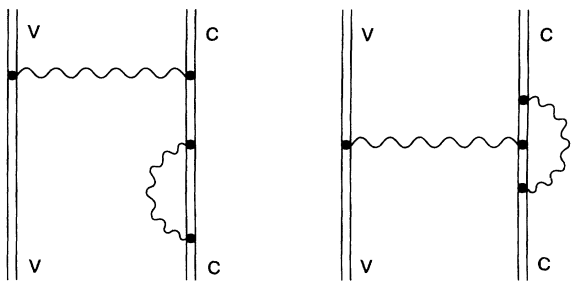

FIG. 6. Typical leading Feynman diagrams for the "core-relaxation" contribution to the self-energy.

TABLE IV. Screened self-energy and Uehling terms for the $2s$ and $2p_{1/2}$ states in lithiumlike U ($Z = 92$) with a finite nucleus. Units are eV.

Term	Energy		
	$2s$	$2p_{1/2}$	$2p_{1/2}$-$2s$
Zero potential	−246.78	−284.55	−37.77
One potential	188.62	169.01	−19.61
Many potential			
$L = 0$	104.26	0.83	−103.43
$L = 1$	10.14	113.74	103.60
$L = 2$	3.26	5.65	2.39
$L = 3$	1.35	1.87	0.52
$L = 4$	0.66	0.80	0.14
$L = 5$	0.37	0.41	0.04
$L = 6$	0.22	0.24	0.01
$L = 7$	0.14	0.15	0.00
$L = 8$	0.09	0.10	0.00
$L = 9$	0.07	0.07	0.00
$L = 10 - \infty$	0.24	0.23	0.00
Total many potential	120.80(6)	124.09(6)	3.28(1)
Total SE	62.64(6)	8.54(6)	−54.09(1)
Uehling	−15.73	−2.61	13.12

agrees well with that of Cheng, Johnson, and Sapirstein [15], 1.88(20) eV, but disagrees by five experimental standard deviations with the value 2.24 eV found by Indelicato and Mohr [14]. Perhaps this discrepancy is due to these authors' linear treatment of the screening potential, as opposed to our all-order treatment, but this seems unlikely since the screening correction is only −3% of the total self-energy. To examine this discrepancy further, we have separated the screening effect for the transition into individual contributions from the $2s$ and $2p_{1/2}$ states, finding −2.75(2) eV and −0.97(2) eV, respectively, compared to −2.88 eV and −0.64 eV of Indelicato and Mohr. The bulk of the discrepancy thus lies in the $2p_{1/2}$ value.

Note that the hydrogenic calculations that we have used above to extract finite-size and screening corrections cancel identically upon adding together all contributions. The final result is controlled entirely by the calculation in Table IV.

A complete tabulation of all effects for this transition is given in Table V. The RMBPT value is that of Blundell, Johnson, and Sapirstein [10], and includes a gross nuclear-finite-size correction based on the nuclear parameters of Zumbro *et al.* [35]. Our nuclear recoil correction differs slightly from the value −0.03 eV given in Ref. [10], because we construct the nuclear kinetic energy operator

TABLE V. Summary of correlation, QED, and nuclear effects for the $2s$ and $2p_{1/2}$ states in lithiumlike U ($Z = 92$). The values are our calculations unless stated explicitly otherwise. SE, self-energy; Uehl., Uehling; FS, nuclear-finite-size correction; HO, two-loop radiative corrections. Units are eV.

Effect	Energy			
	$2s$	$2p_{1/2}$	$2p_{1/2}$-$2s$	Other
RMBPT[a]			322.41	
Nucl. recoil			−0.08(8)	
Nucl. polarization[b]			0.18(5)	
Pt. nuc. hyd. SE[c]	66.30	9.63	−56.67	
SE-FS	−0.98(6)	−0.12(5)	0.80(1)	1.0(1),[d] 0.6(2)[e]
Valence screening (SE)	−2.75(2)	−0.97(2)	1.77(1)	2.24,[f] 1.88(20)[e]
Core relaxation (SE)			0.23(1)	0.27[f]
Total self-energy			−53.87(2)	
Pt. nuc. hyd. Uehl.[d]	−17.31	−3.00	14.31	
Uehl.-FS	0.85	0.09	−0.76	−0.76[d]
Valence screening (Uehl.)	0.73	0.29	−0.44	−0.44[e]
Core relaxation (Uehl.)			−0.08	
Wichmann-Kroll[g]	0.79	0.18	−0.60	
Total vac. pol.			12.44	
HO[h]	−0.02(4)	−0.02(1)	0.01(4)	
Total QED			−41.43(4)	
Total theory			281.08(10)	
Experiment[i]			280.59(9)	

[a] From Ref. [10].
[b] From Ref. [37].
[c] Reference [2].
[d] From Ref. [33].
[e] Reference [15].
[f] Reference [14].
[g] From Refs. [33] and [34] with scaling (see text).
[h] From Refs. [33] and [38].
[i] Reference [4].

from the momentum operator $\mathbf{p} = -i\nabla$ instead of the operator $\mathbf{p} = c\boldsymbol{\alpha}$ used in that reference. Owing to the uncertainty in relativistic corrections to nuclear recoil, we assign an error equal to the value of the term. The nuclear polarization term has been evaluated by Plunien *et al.* [37]. The "core-relaxation" contribution to the self-energy is a two-experimental-standard-deviation effect, and agrees quite well with the estimate of Indelicato and Mohr [14]. The Wichmann-Kroll terms include a very small −3% estimate of screening, in analogy with the screening to the Uehling term. The "higher-order" (HO) term consists of the second-order radiative corrections for the hydrogenic ion, evaluated to leading order in $Z\alpha$. We modify the value tabulated in Ref. [33] to incorporate the more accurate evaluation of the order $\alpha^2(Z\alpha)$ vacuum-polarization (or Källén-Sabry) terms by Beier and Soff [38] and Indelicato and Desclaux [32]. The error estimate for the HO terms reflects uncertainty in corrections of higher order in $Z\alpha$, and is in accordance with Ref. [33].

We present an analysis of the Na-like and Cu-like transitions in Table VI. In these multishell ions, the majority of the small core-relaxation contribution to the self-energy, about 90%, comes from the $1s$ states. We find a rather large screening effect on the self-energy, about 20% for the Na-like, and 45% for the Cu-like transition. The Na-like screened self-energy agrees well with that of Cheng, Johnson, and Sapirstein [15], −6.83(10) eV. We also find very good agreement with the phenomenological QED calculations described by Kim *et al.* [11], who give −5.29 eV for the total QED in the Na-like transition, and −2.12 eV for the Cu-like transition.

TABLE VI. Correlation and screened QED effects for transitions in Na-like Pt and Cu-like Bi. For acronyms, see the caption to Table V. Units are eV.

Effect	Energy	
	Na-like Pt $3p_{3/2}$-$3s$	Cu-like Bi $4p_{1/2}$-$4s$
RMBPT[a]	658.76[b]	122.84[c]
SE(valence)	−6.80	−2.63
SE(core)	0.07(1)	0.01
Self-energy	−6.73(1)	−2.62
Uehl.(valence)	1.50	0.54
Uehl.(core)	−0.02	0.00
WK[d]	−0.06	−0.02
Vacuum polarization	1.43	0.52
HO[e]	0.00	0.00
Total QED	−5.30(1)	−2.11
Total	653.45(1)	120.73
Experiment	653.44(7)	120.90(2)

[a] Includes nuclear recoil term.
[b] Reference [8].
[c] Reference [9].
[d] References [33] and [34] with scaling (see text).
[e] References [33] and [38] with $1/n^3$ scaling.

V. DISCUSSION AND CONCLUSIONS

What we have presented in this paper is a practical procedure for performing calculations of the self-energy for high-Z ions in a numerically specified, non-Coulombic, local potential. For transitions in systems with $Z > 70$, the method readily achieves accuracies of better than 0.01 eV, while the typical experimental precision is ≥ 0.02 eV in this region. As such, the method represents one solution to the problem of understanding both nuclear-finite-size and screening corrections to the self-energy in high-Z ions in a rigorous QED framework.

The crucial difference between this method and earlier ones is the separate treatment of the one-potential term. We have shown that the removal of the one-potential term from the configuration-space part of the calculation accelerates the convergence of the partial-wave expansion, and that if one considers the transition directly, only a few partial waves need be summed explicitly. This simplicity permits an accurate evaluation of the self-energy for an arbitrary local potential having no special analytic properties.

As noted earlier [18], the cancellation of large, spurious, gauge-dependent terms between the zero-, one-, and many-potential terms reduces the accuracy of the algorithm, particularly at low Z or for states with high angular momentum. Here we have avoided this problem partly by making use of systematic cancellations of the spurious terms between two states in a transition, achieving high accuracy with relatively few basis functions. For precise calculations at low Z, however, it may be desirable to improve the algorithm itself, rather than refine the numerical techniques. Such an improvement may result by using either the Fried-Yennie [39, 16] or Coulomb gauge in which the spurious terms are absent. Our preliminary calculations of the many-potential term in Coulomb gauge not only follow the physical Z^4 scaling, but suggest an additional useful feature, that the many-potential term is a small fraction of the total self-energy.

Now that accurate calculations of the one-photon self-energy and vacuum polarization are possible in realistic potentials at high Z, the focus of attention shifts to the uncalculated QED effects in two-photon diagrams. Probably most important among these are the exchange variants of the basic screening diagrams (Fig. 7), and certain terms from the box and crossed-box diagrams (Fig. 8) that have been omitted from the RMBPT work. Specifically, these omitted terms involve effects in which negative-energy states enter the internal electron propagators, a correct treatment of retardation terms from these diagrams, and the two-transverse-photon-exchanged terms. We believe that basis-set techniques, similar to those used for the many-potential term in the present work, will prove useful in this work.

Turning now to the results for Li-like U, the agreement we find between theory and experiment is acceptable, since the omitted terms discussed above are expected to

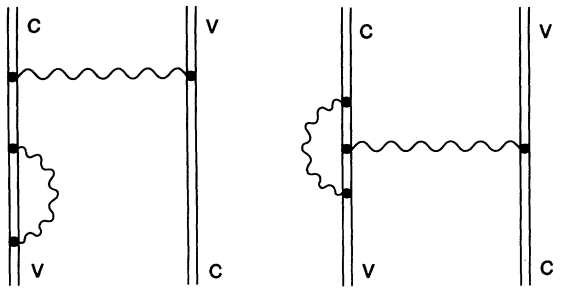

FIG. 7. Sample exchange variants of the valence screening diagrams.

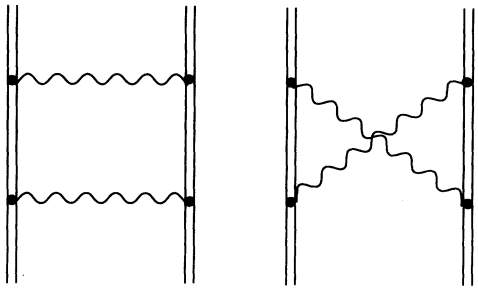

FIG. 8. Box and crossed-box diagrams.

enter at this level. We expect that inclusion of these terms should bring theory and experiment into agreement at the 0.1 eV level. To understand the transition energy to better than this will require a better understanding of relativistic corrections to the nuclear recoil term in many-electron systems. The recoil term for the transition is dominated by the mass-polarization effect, which is not present for one-electron systems. Also entering at this level are two-loop radiative corrections, so far known only to leading order in $Z\alpha$. In analogy to the one-photon self-energy, it is possible that some of these corrections become nonperturbative in $Z\alpha$ at high Z. Finally, one will have to examine critically the error present in the estimate of nuclear polarization.

The agreement with experiment found in Na-like Pt is good, but may be fortuitous pending a more careful study of the omitted two-photon terms. The agreement in Cu-like Bi is rather poor, however. The Na-like and Cu-like results seem inconsistent because if the omitted terms are small in the Na-like transition, they are unlikely to account for the discrepancy in the Cu-like transition. In their recent systematic study of Cu-like ions involving a smoothed fit to the difference of theory and experiment, Kim *et al.* [11] concluded that the measured value for Cu-like Bi is probably too high. Their predicted transition energy of 120.73 eV is in excellent agreement with our theory.

In summary, we believe that accurate screened self-energy and vacuum-polarization calculations of the type described in this paper are sufficient to account for the QED contributions to the structure of high-Z ions to a few tenths of an eV. Inclusion of a few well-defined higher-order terms should improve the theory further.

Note added in proof. We have recently learned that Mohr and Soff [40] have calculated the $2p_{1/2}$-$2s$ self-energy for H-like U with two finite nuclear models: a spherical shell and a uniformly charged sphere. Their results agree closely with our value given in Table III when they use the same rms nuclear radius. Another calculation by Cheng, Johnson, and Sapirstein [41] also agrees closely.

ACKNOWLEDGMENTS

I would like to thank Neal Snyderman for many valuable discussions and encouragement, and also to acknowledge helpful discussions with K. T. Cheng, Paul Indelicato, Walter Johnson, Jonathan Sapirstein, and Bernard Zygelman. The work was performed under the auspices of the U.S. Department of Energy by Lawrence Livermore National Laboratory under Contract No. W-7405-Eng-48.

APPENDIX A: FEYNMAN-GAUGE PHOTON INTERACTION MATRIX ELEMENT

We infer the form for the generalized Slater integral $R_L(\omega; abcd)$ from Appendix B of Ref. [7]. Replacing the frequency-independent radial Green's function $r_<^L/r_>^{L+1}$ by the frequency-dependent one,

$$g_L(\omega; r, r') = i\frac{\omega}{c}(2L+1)j_L(\omega r_</c)h_L^{(1)}(\omega r_>/c), \qquad \text{(A1)}$$

in Eqs. (B11) and (B12) of that reference, we obtain

$$\begin{aligned} R_L(\omega; abcd) = (-1)^L C_L(ac)C_L(bd)\Bigg[& \int_0^\infty dx \int_0^\infty dy\, g_L(\omega; x, y) W_{ac}(x) W_{bd}(y) \\ & + \frac{L+1}{2L+3}\int_0^\infty dx \int_0^\infty dy\, g_{L+1}(\omega; x, y) Q_{ac}(x) Q_{bd}(y) \\ & + \frac{L}{2L-1}\int_0^\infty dx \int_0^\infty dy\, g_{L-1}(\omega; x, y) P_{ac}(x) P_{bd}(y)\Bigg] \\ & + (-1)^{L+1} C_L(-ac)C_L(-bd)\frac{(\kappa_a+\kappa_c)(\kappa_b+\kappa_d)}{L(L+1)}\int_0^\infty dx \int_0^\infty dy\, g_L(\omega; x, y) V_{ac}(x) V_{bd}(y). \end{aligned} \qquad \text{(A2)}$$

Here

$$P_{ac}(x) = U_{ac}(x) - \frac{\kappa_a - \kappa_c}{L} V_{ac}(x), \tag{A3}$$

$$Q_{ac}(x) = -U_{ac}(x) - \frac{\kappa_a - \kappa_c}{L+1} V_{ac}(x), \tag{A4}$$

$$U_{ac}(x) = g_a(x) f_c(x) - f_a(x) g_c(x), \tag{A5}$$

$$V_{ac}(x) = g_a(x) f_c(x) + f_a(x) g_c(x), \tag{A6}$$

$$W_{ac}(x) = g_a(x) g_c(x) + f_a(x) f_c(x). \tag{A7}$$

The quantity $C_L(ab) = \langle \kappa_a \| C^L \| \kappa_b \rangle$ is a reduced matrix element of C^L, while $C_L(-ab)$ is $C_L(ab)$ with κ_a replaced by $-\kappa_a$.

Note that the above formula applies when the sign of the square root in (9) is positive, which is appropriate for real, positive values of ω (generally, above the branch cuts in the upper-half plane in Fig. 4). For the other branch, one must reverse the sign of ω in the right-hand side of (A2).

APPENDIX B: INTEGRATION SCHEME FOR ONE-POTENTIAL TERM

We consider here the numerical evaluation of the integral

$$I \equiv \int_0^\infty dp_1 \int_0^\infty dp_2 \int_{-1}^{1} dz \, \frac{1}{q^2} f(p_1, p_2, z), \tag{B1}$$

where $p_1 = |\mathbf{p}_1|$, $p_2 = |\mathbf{p}_2|$, and $q^2 = |\mathbf{p}_1 - \mathbf{p}_2|^2 = p_1^2 + p_2^2 - 2p_1 p_2 z$. With the change of variables

$$v = -\frac{1}{2p_1 p_2} \ln(q^2), \tag{B2}$$

$$x = p_1 + p_2, \tag{B3}$$

$$y = p_1 - p_2, \tag{B4}$$

and use of the symmetry of the integral under $y \to -y$, the integral becomes

$$I = 4 \int_0^\infty dx \int_0^x dy \int_{v_{\min}}^{v_{\max}} dv \, f\left(\frac{x+y}{2}, \frac{x-y}{2}, z(x,y,v) \right), \tag{B5}$$

$$v_{\min} = -\frac{1}{p_1 p_2} \ln(x), \tag{B6}$$

$$v_{\max} = -\frac{1}{p_1 p_2} \ln(y). \tag{B7}$$

This expression still contains a logarithmic singularity in the y integration as $y \to 0$, which we remove with the further substitution

$$s = y \ln(y/x) - y, \tag{B8}$$

for y in the range $0 \le y \le x/10$. Having transformed the expression into this form, we use Gauss-Legendre integration with the infinite x integration mapped to a finite range by an inverse-tangent substitution.

* Present address: DRFMC/LIAA, Centre d'Etudes Nucl. de Grenoble, B.P. 85X, 38041 Grenoble CEDEX, France.

[1] P. J. Mohr, Ann. Phys. (N.Y.) **88**, 26 (1974); **88**, 52 (1974).

[2] P. J. Mohr, Phys. Rev. Lett. **34**, 1050 (1975); Phys. Rev. A **26**, 2338 (1982); this issue, **46**, 4421 (1992).

[3] P. J. Mohr and Y.-K. Kim, Phys. Rev. A **45**, 2727 (1992).

[4] J. Schweppe, A. Belkacem, L. Blumenfeld, N. Claytor, B. Feinberg, H. Gould, V. E. Kostroun, L. Levy, S. Misawa, J. R. Mowat, and M. H. Prior, Phys. Rev. Lett. **66**, 1434 (1991).

[5] T. E. Cowan, C. L. Bennett, D. D. Dietrich, J. Bixler, C. J. Hailey, J. R. Henderson, D. A. Knapp, M. A. Levine, R. E. Marrs, and M. B. Schneider, Phys. Rev. Lett. **66**, 1150 (1991).

[6] J. F. Seely, J. O. Ekberg, C. M. Brown, U. Feldman, W. E. Behring, J. Reader, and M. C. Richardson, Phys. Rev. Lett. **57**, 2924 (1986).

[7] W. R. Johnson, S. A. Blundell, and J. Sapirstein, Phys. Rev. A **37**, 2764 (1988).

[8] W. R. Johnson, S. A. Blundell, and J. Sapirstein, Phys. Rev. A **38**, 2699 (1988).

[9] W. R. Johnson, S. A. Blundell, and J. Sapirstein, Phys. Rev. A **42**, 1087 (1990).

[10] S. A. Blundell, W. R. Johnson, and J. Sapirstein, Phys. Rev. A **41**, 1698 (1990).

[11] Y.-K. Kim, D. H. Baik, P. Indelicato, and J. P. Desclaux, Phys. Rev. A **44**, 148 (1991).

[12] A. M. Desiderio and W. R. Johnson, Phys. Rev. A **3**, 1287 (1971).

[13] G. E. Brown, J. S. Langer, and G. W. Schaefer, Proc. R. Soc. London Ser. A **251**, 92 (1959).

[14] P. Indelicato and P. J. Mohr, in *Atomic Physics 12*, Proceedings of Papers on Trapping of Neutral Atoms, History of ICAP, and Tests of Symmetries, edited by Jens C. Zorn and Robert R. Lewis, AIP Conf. Proc. No. 233 (AIP, New York, 1990); Theor. Chim. Acta **80**, 207 (1991).

[15] K. T. Cheng, W. R. Johnson, and J. Sapirstein, Phys. Rev. Lett. **66**, 2960 (1991).

[16] N. J. Snyderman, Ann. Phys. (N.Y.) **211**, 43 (1991).

[17] M. Baranger, H. A. Bethe, and R. P. Feynman, Phys. Rev. **92**, 482 (1953).

[18] S. A. Blundell and N. J. Snyderman, Phys. Rev. A **44**, R1427 (1991).

[19] J. Sapirstein, Phys. Scr. **36**, 801 (1987).

[20] S. S. Schweber, *An Introduction to Relativistic Quantum Field Theory* (Harper and Row, New York, 1961).

[21] C. Itzykson and J.-B. Zuber, *Quantum Field Theory* (McGraw-Hill, New York, 1985).

[22] P. J. Mohr, in *Relativistic, Quantum Electrodynamic, and*

Weak Interaction Effects in Atoms, Proceedings of the Program Held on Relativistic, Quantum Electrodynamic, and Weak Interaction Effects in Atoms at the Institute of Theoretical Physics, Santa Barbara, CA, 1988, edited by W. R. Johnson, P. J. Mohr, and J. Sucher, AIP Conf. Proc. No. 189 (AIP, New York, 1988).
[23] J. D. Jackson, *Classical Electrodynamics*, 2nd ed. (Wiley, New York, 1975), p. 742.
[24] D. M. Brink and G. R. Satchler, *Angular Momentum*, 2nd ed. (Clarendon, Oxford, 1968).
[25] E. A. Uehling, Phys. Rev. **48**, 55 (1935).
[26] R. Serber, Phys. Rev. **48**, 49 (1935).
[27] P. Indelicato and E. Lindroth, Phys. Rev. A (to be published).
[28] S. A. Blundell, W. R. Johnson, and J. Sapirstein, Phys. Rev. A **37**, 307 (1988).
[29] C. deBoor, *A Practical Guide to Splines* (Springer, New York, 1978).
[30] J. F. Seely, Phys. Rev. A **39**, 3682 (1989).
[31] J. F. Seely and R. A. Wagner, Phys. Rev. A **41**, 5246 (1990).
[32] P. Indelicato and J. P. Desclaux, Phys. Rev. A **42**, 5139 (1990).
[33] W. R. Johnson and G. Soff, At. Data Nucl. Data Tables **33**, 405 (1985).
[34] G. Soff and P. J. Mohr, Phys. Rev. A **38**, 5066 (1988).
[35] J. D. Zumbro, E. B. Shera, Y. Tanaka, C. E. Bemis, Jr., R. A. Naumann, M. V. Hoehn, W. Reuter, and R. M. Steffen, Phys. Rev. Lett. **20**, 1888 (1984).
[36] K. T. Cheng, W. R. Johnson, and J. Sapirstein (private communication).
[37] G. Plunien, B. Müller, W. Greiner, and G. Soff, Phys. Rev. A **39**, 5428 (1989); **43**, 5853 (1991).
[38] T. Beier and G. Soff, Z. Phys. D **8**, 129 (1988).
[39] H. M. Fried and D. R. Yennie, Phys. Rev. Lett. **4**, 583 (1960); Phys. Rev. **112**, 1391 (1958).
[40] P. J. Mohr and G. Soff (private communication).
[41] K. T. Cheng, W. R. Johnson, and J. Sapirstein (private communication).